

Numerical approximation of a neural field model with 2 populations in 1 and 2 Dimensions

Guilherme Brás

guilherme.bras@tecnico.ulisboa.pt

December 2024

Abstract

This extended abstract outlines the research conducted on numerical approximations of neural field systems, focusing primarily on the development of a two-field model. This model captures the dynamic interactions of coupled neuronal populations influenced by various external stimuli. The methodology involves advanced numerical techniques, specifically Fast Fourier Transforms (FFTs), to effectively solve the integro-differential equations governing these systems, thereby providing significant insights into neural dynamics and their interactions.

1 Introduction

The human brain, an extraordinary biological information processor, comprises billions of neurons whose interactions underpin complex cognitive functions. Traditional models often focus on detailed neuronal interactions, offering limited insights into large-scale neural dynamics. A shift towards macroscopic descriptions, like neural field theory [1, 2], is crucial for capturing essential features of large-scale brain activity. This theory simplifies these interactions through a continuous field representation, expressed by the integro-differential equation:

$$\frac{\partial u(x, t)}{\partial t} = I(x, t) - u(x, t) + \int_{\Omega} w(|x - y|) f(u(y, t)) dy \quad (1)$$

This model accounts for local excitation and long-range inhibition observed in cortical networks, as extensively studied by Coombes [3], demonstrating its applicability in analyzing waves and patterns in neural activity.

Deterministic models sometimes overlook the stochastic nature of brain activity. Introducing stochastic elements, as Killpatrick and Ermentrout [4] have explored, enriches this depiction with the stochastic neural field equation:

$$du(x, t) = \left(I(x, t) - u(x, t) + \int_{\Omega} w(|x - y|) f(u(y, t)) dy \right) dt + \sigma dW(x, t) \quad (2)$$

Kuehn and Riedler [5] and Sequeira [6] further expand our understanding by analyzing noise influences on neural dynamics, which are crucial for cognitive functions like working memory.

Single-field models, as noted by Amari [1], can inadequately capture complex stimuli responses, leading to the development of advanced models such as the two-field model [7], described by:

$$\begin{cases} \frac{\partial u(x,t)}{\partial t} = I(x,t) - u(x,t) + v(x,t) + \int_{\Omega} w(|x-y|)f(u(y,t),\theta)dy \\ \tau_v \frac{\partial v(x,t)}{\partial t} = u(x,t) - v(x,t) - \int_{\Omega} w(|x-y|)f(u(y,t),\theta)dy \end{cases} \quad (3)$$

This model integrates adaptive dynamics, capturing a broader range of neural behaviors, such as robust working memory patterns, as shown by Wojtak et al [8, 9]. The two-field architecture showcases enhanced capabilities in replicating sustained neural responses and cognitive processes under varying stimuli. Exploring these models through robust numerical methods [10, 11] facilitates comprehensive analysis of neural systems.

In summary, advancing models beyond traditional neural field equations by incorporating stochasticity and adaptive dynamics holds promise for improved representations of neural functions, with implications for neuroscience and artificial intelligence applications.

2 Approximation in 1 Dimension

We begin by approximating the solution for the case where $\Omega \subset \mathbb{R}^1$ and $\Omega = [-L, L]$.

To discretize the time and space domains, we divide the time interval into small steps of size Δt and the spatial domain into small steps of size Δx . The time derivatives are approximated using a forward difference approximation, yielding:

$$\begin{cases} \frac{u(x,t_{i+1})-u(x,t_i)}{\Delta t} = I(x,t_i) - u(x,t_i) + v(x,t_i) + \int_{\Omega} w(|x-y|)f(u(y,t_i),\theta) dy \\ \tau_v \frac{v(x,t_{i+1})-v(x,t_i)}{\Delta t} = u(x,t_i) - v(x,t_i) - \int_{\Omega} w(|x-y|)f(u(y,t_i),\theta) dy \end{cases} \quad (4)$$

Next, we apply the Trapezium rule to approximate the integral in our discretized domain for each t_i :

$$\int_{\Omega} w(|x-y|)f(u(y,t_i),\theta) dy \approx 2\Delta x \left[w(|x+L|)f(u(-L,t_i),\theta) + w(|x-L|)f(u(L,t_i),\theta) + 2 \sum_{j=1}^{N-1} w(|x+L-jh|)f(u(jh-L,t_i),\theta) \right] \quad (5)$$

To simplify notation, we denote the right-hand side of this equation as $Integral(x,t_i)$. Using this, we can update the values of u and v at each time step:

$$\begin{cases} u(x,t_{i+1}) = (1 - \Delta t)u(x,t_i) + \Delta t(I(x,t_i) + v(x,t_i)) + \frac{\Delta t \Delta x}{2} Integral(x,t_i) \\ v(x,t_{i+1}) = (1 - \frac{\Delta t}{\tau_v})v(x,t_i) + \frac{\Delta t}{\tau_v}u(x,t_i) - \frac{\Delta t \Delta x}{2\tau_v} Integral(x,t_i) \end{cases} \quad (6)$$

For simplicity, we will use $\tau_v = 1$, which leads us to the relationship:

$$u(x,t_{i+1}) + v(x,t_{i+1}) = u(x,t_i) + \Delta t I(x,t_i) + v(x,t_i). \quad (7)$$

This holds for all $i \geq 0$. In scenarios where no external inputs act on the system ($I(x,t_i) = 0$), we

have the initial condition $u(x, t_i) + v(x, t_i) = K(x)$.

2.1 Scenarios for Numerical Approximations

Gaussian functions are the simplest model for approximating connectivity in working memory studies. They reflect the property of local connectivity, where connections are strongest between nearby neurons, decreasing with distance. Their bell-shaped curve assigns the highest weights to nearby neurons while remaining smooth and differentiable, facilitating mathematical analysis.

We model the weight function to represent how connections are formed based on the distances between neurons. Additionally, Gaussian functions can represent external inputs applied to the neural system, centered around specific locations and modulated by amplitude and duration.

The firing rate function utilized in our model is based on a threshold mechanism, where the response of the neural population is activated when the input exceeds a certain firing threshold.

To obtain comparable results to the one-field model, we employ three scenarios for our numerical experiments, ensuring they maintain the property $u(x, 0) + v(x, 0) = K(x)$:

1. $u(x, 0) = A_u e^{\left(-\frac{x^2}{2\sigma_u^2}\right)}, \quad v(x, 0) = K - u(x, 0), \quad I(x, t) = 0$

In this scenario, $A_u, \sigma_u > 0$ and $K \geq 0$ is constant, initializing u with a Gaussian function.

2. $u(x, 0) = K(x), \quad v(x, 0) = 0, \quad K(x) = A_k e^{\left(-\frac{x^2}{2\sigma_k^2}\right)}, \quad I(x, t) = 0$

Here, $A_k, \sigma_k > 0$. The initial values for v are all set to zero, while u is defined by a Gaussian function.

3. $u(x, 0) = v(x, 0) = K(x) = 0, \quad I(x, t)$ defined as a sum of Gaussian functions

This is the only scenario with external inputs applied to the system.

2.2 Results

The figures below illustrate the results for u (solid lines) and v (dotted lines) with $\Delta t = 0.05$, $\Delta x = 0.05$, and $L = 10$. Using kernel parameters $A_{ex} = 2$, $\sigma_{ex} = 1.25$, $A_{in} = 1$, $\sigma_{in} = 2.5$, and $\omega_{inh} = 0.1$:

We conducted tests using Scenarios 1 and 2 to validate the functionality of the system. However, since the primary objective is to assess its ability to preserve the characteristics of external stimuli, we will now explore how these inputs interact with the system by examining Scenario 3. The results of this analysis are depicted in Figure 1 as well as in Table 1 where you can see the Activity domain diameter (ADD) of both I and u and the maximum value u attains.

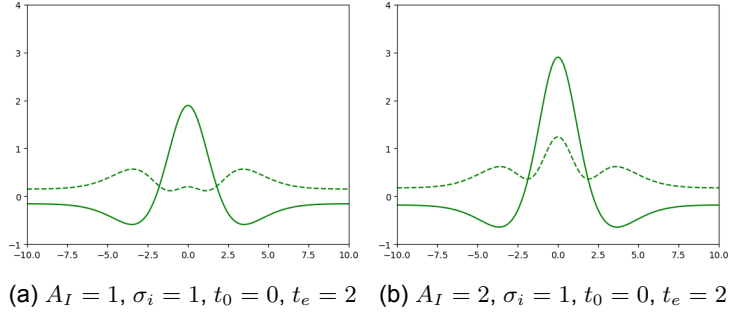


Figure 1: Results using the model in 1 Dimension at $t = T = 10$ for scenario 3, with different external inputs centered at $x_c = \{0\}$ acting independently, $\theta = 0.5$

	$A_I = \{1\}$	$A_I = \{1.5\}$	$A_I = \{2\}$	$A_I = \{2.5\}$
ADD of $I(x, t)$	2.3	2.9	3.3	3.5
ADD of $u(x, t)$	3.0	3.3	3.5	3.65
Maximum value of $u(x, t)$	1.8944	2.4016	2.9018	3.4008

Table 1: Scenario 3 using the model in 1D with different values for A_I

The results displayed in Figure 1 elucidate the impact of varying external stimuli on the dynamics of the neural population. As indicated in Table 1, increasing the amplitude of the external input $I(x, t)$ significantly enhances the maximum values of $u(x, t)$ and leads to a broader activity domain. For instance, the comparison of scenarios in subfigures 1b and 1a illustrates how a greater amplitude results in heightened activity within the neural field.

	$\sigma_I = \{1\}$	$\sigma_I = \{3\}$	$\sigma_I = \{6\}$	$\sigma_I = \{10\}$
ADD of $I(x, t)$	2.3	7	14.1	20
ADD of $u(x, t)$	3.0	5.2	7.2	8.55
Maximum value of $u(x, t)$	1.8944	1.5842	1.1782	1.0808

Table 2: Scenario 3 using the model in 1D with different values for σ_I

Furthermore, Table 2 demonstrates that when the spread of the external input is increased, as seen in scenario 3's application of σ_I , the activity domain of $u(x, t)$ also widens considerably, while the maximum response remains stable. This suggests that a wider external input can effectively engage more neurons without overwhelming the system's activity levels.

	$t_e = 2$	$t_e = 3$	$t_e = 4$	$t_e = 5$
ADD of $I(x, t)$	2.3	2.3	2.3	2.3
ADD of $u(x, t)$	3.0	3.3	3.5	3.7
Maximum value of $u(x, t)$	1.8944	2.4278	2.9287	3.4234

Table 3: Scenario 3 using the model in 1D with different values for t_e

In summary, the analysis of Figure 1 in conjunction with the data presented in Tables 1 - 3 underscores the two-field model's improved capacity to capture the nuances of neural responses to varying strengths and distributions of inputs, a significant advancement over the single-field model that fails to encapsulate these dynamics accurately.

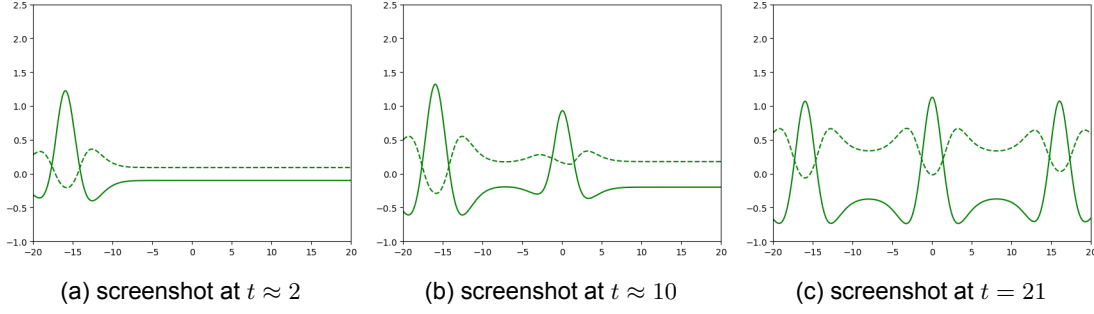


Figure 2: Results obtained using the 1D model from applying three different external inputs with a duration of 1s, at times $t_1 = 1$, $t_2 = 9$, $t_3 = 18$. $A_I = \{1, 1, 1\}$, $\sigma_I = \{1, 1, 1\}$, $x_c = \{-16, 0, 16\}$, $\theta = 0.4$

Figure 2 illustrates the model's ability to retain information from multiple external stimuli, showcasing its advanced capability over the single-field model. The system accurately identifies and preserves the characteristics of the external stimuli applied. This advancement is particularly relevant in studies concerning working memory and robotics, where understanding the characteristics of stimuli with high fidelity is essential.

3 Two-field Model with Piecewise Linear Feedback

In neural interactions, feedback is often not directly proportional to the source potential. It tends to grow when the potential of the source field is within a certain interval $[0, k]$ and remains constant when outside this interval. Given this behavior, it is reasonable to replace the feedback term v in the first equation of system 3 with $g(v, k)$ and similarly replace u with $g(u, k)$ in the second equation. Here, g is a continuous function that captures this behavior, and k is a positive number that defines the range within which the feedback intensity changes.

In this context, we modify system 3 to yield the following equations:

$$\begin{cases} \frac{\partial u(x,t)}{\partial t} = I(x,t) - u(x,t) + g(v(x,t), k) + \int_{\Omega} w(|x-y|)f(u(y,t), \theta)dy \\ \tau_v \frac{\partial v(x,t)}{\partial t} = g(u(x,t), k) - v(x,t) - \int_{\Omega} w(|x-y|)f(u(y,t), \theta)dy \end{cases} \quad (8)$$

Where the function $g(u, k)$ is defined for $k \in \mathbb{R}^+$ as:

$$g(u, k) = \begin{cases} 0, & u < 0 \\ \frac{1}{k}u, & 0 \leq u \leq k \\ 1, & u > k \end{cases} \quad (9)$$

This section aims to analyze how the behavior of solutions of 8 differs from those of 3. To accomplish this, we reproduce several numerical experiments from Sections 1 and 2, using the modified model 8 with varying values of k .

Old model $\backslash A_I =$	{0.5}	{0.7}	{0.9}	{1}	{2}	{3}	{4}
ADD of $I(x,t)$	0.0	1.6	2.1	2.3	3.3	3.7	4.0
ADD of $u(x,t)$	0.0	2.3	2.5	2.5	3.0	3.3	3.5
Max of $u(x,t)$	0.2558	1.1732	1.3013	1.3524	1.8932	2.3996	2.8993

New model with $k = 1$ $A_I =$	{0.5}	{0.7}	{0.9}	{1}	{2}	{3}	{4}
ADD of $I(x, t)$	0.0	1.6	2.1	2.3	3.3	3.7	4.0
ADD of $u(x, t)$	0.0	2.65	2.65	2.65	2.65	3.3	3.5
Max of $u(x, t)$	0.2558	1.6646	1.6661	1.6663	1.6967	1.6869	1.6637

New model with $k = 1.5$ $A_I =$	{0.5}	{0.7}	{1.1}	{1.5}	{2}	{3}	{4}
ADD of $I(x, t)$	0.0	1.6	2.5	2.9	3.3	3.7	4.0
ADD of $u(x, t)$	0.0	0.0	2.65	2.7	2.7	2.7	2.7
Max of $u(x, t)$	0.0098	0.0138	1.6663	1.6740	1.6741	1.6743	1.6746

New model with $k = 2$ $A_I =$	{0.7}	{0.8}	{1.2}	{1.8}	{2}	{3}	{4}
ADD of $I(x, t)$	1.6	1.9	2.6	3.2	3.3	3.7	4.0
ADD of $u(x, t)$	0	2.65	2.65	2.7	2.7	2.7	2.7
Max of $u(x, t)$	0.0027	1.6657	1.6663	1.6741	1.6742	1.6744	1.6746

Table 4: Characteristics of the stabilized solutions in the case of $t_0 = 0$, $t_e = 1$, $\sigma_I = \{1\}$, $x_c = \{0\}$, $\theta = 0.5$, for different A_I in the models with and without saturation

When examining the new model, it is essential to analyze its behavior compared to the original model. Table 4 presents data that illustrates why this model may not adequately preserve the characteristics of external inputs. In particular, when the signal intensity nears the threshold k , the modified model fails to generate a consistent bump shape in the resulting profiles, indicating that the model is overly rigid.

Table 4 shows that when the input intensity is low (e.g., $A_I = 0.5$), the old model produces a strong response, while the new model struggles to yield a similar result. The presence of a bump in the old model's output signifies an adaptive response to the initial conditions, which is compromised in the new model due to its piecewise linear nature in feedback representation.

Moreover, as evident from the table, for sufficiently high input intensities (such as $A_I = 1$), both models produce bumps; however, the new model with lower k values exhibits greater fluctuations in the shape of these profiles. This underscores the limitation of maintaining response fidelity in the modified system under specific parameter settings.

In conclusion, while the model with piecewise linear feedback introduces realism, it can lead to a loss in sensitivity regarding the characteristics of the input signals. The balance between parameter k and the model's response to external stimuli is critical for achieving accurate representations of neural dynamics.

4 Approximations in 2D

We now aim to numerically approximate the system of equations describing the dynamics of potentials $u(x, t)$ and $v(x, t)$ over the domain $\Omega = [-L/2, L/2]^2$. As Sequeira did in his thesis [6] we'll handle convolution terms using the Fast Fourier Transform (FFT) for computational efficiency.

The spatial domain Ω is discretized into a uniform grid with spacing Δx , and time is discretized using a step size Δt . Similar to our one-dimensional approximations, we employ the explicit Euler method to discretize the temporal derivatives, leveraging the FFT for computations in the frequency domain. This approach significantly enhances computational efficiency in managing the convolution terms inherent in our neural field equations.

To derive the numerical solutions, we utilize the continuous Fourier transform, defined as:

$$\mathcal{F}\{g\} = \int_{\Omega} g(\mathbf{x}) e^{-i\mathbf{k}_{mn} \cdot \mathbf{x}} d\mathbf{x} \quad (10)$$

Here, \mathbf{k}_{mn} is the wave vector defined by $\mathbf{k}_{mn} = \frac{2\pi}{L}(m, n)$.

We represent $u(\mathbf{x}, t)$ and $v(\mathbf{x}, t)$ using Fourier series expansions, enabling us to reformulate the system equations in terms of Fourier coefficients $\hat{u}_{mn}(t)$ and $\hat{v}_{mn}(t)$. This method simplifies the handling of convolution terms and allows for more straightforward numerical computations.

The equivalent equations for the Fourier coefficients after appropriate manipulations lead to:

$$\frac{d\hat{u}_{mn}(t)}{dt} = \hat{I}_{mn}(t) - \hat{u}_{mn}(t) + \hat{v}_{mn}(t) + \hat{A}_{mn}(t) \quad (11)$$

$$\frac{d\hat{v}_{mn}(t)}{dt} = \frac{1}{\tau_v} \left(\hat{u}_{mn}(t) - \hat{v}_{mn}(t) - \hat{A}_{mn}(t) \right) \quad (12)$$

Where $\hat{A}_{mn}(t)$ represents the Fourier transform of the convolution term, which can be calculated efficiently using FFTs.

When analysing the 2D-model, we have considered scenarios parallel to those of the one-dimensional studies previously discussed. For example, we present results showing stabilized solutions for both u and v at different conditions in Figure 3.

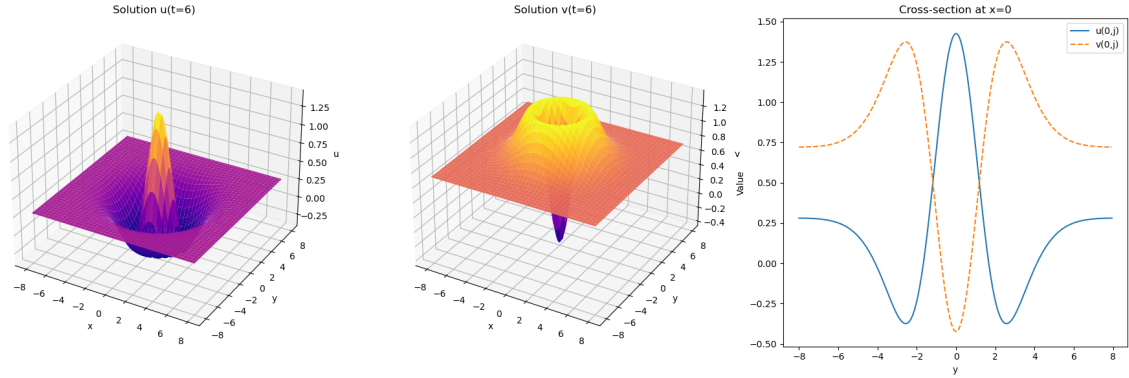


Figure 3: Results obtained using the model in 2D at $t = T = 6$ for scenario 1 with $A_u = 1$, $K = 1$, $\sigma_u = 1$

As shown in Figure 3, the potential dynamics exhibit characteristics that mirror the expected outcomes based on the initial conditions. This further substantiates the model's credibility.

Table 5 indicates that increasing the amplitude of the external input significantly enhances both the activity domain area of u and its maximum value. For instance, the maximum value of u rises from 1.9267 for $A_i = 1$ to 3.3688 for $A_i = 2.5$, demonstrating the model's capacity to effectively respond to variations in the amplitude of applied stimuli.

Additionally, the duration of the external signals substantially impacts the system's response. Different signal durations yield similar stabilized solutions to those observed when varying intensities of the inputs in the same proportion (Tables 5 and 6). This consistency underscores the model's robust sensitivity to both the duration and amplitude of external stimuli, allowing it to maintain proper dynamics across similar signals.

	$A_i = 1$	$A_i = 1.5$	$A_i = 2$	$A_i = 2.5$
Activity Domain Area of I	4.3320	6.8945	8.7227	10.1289
Activity Domain Area of u	4.3633	5.1914	5.8164	6.4414
Maximum value of u	1.9267	2.4306	2.9090	3.3688

Table 5: Characteristics of the stabilized solutions in the case of $t_0 = 0$, $t_e = 2$, $\sigma_I = \{1\}$, $x_c = \{(0,0)\}$, $\theta = 0.5$, for different A_I in 2D

	$t_e = 2$	$t_e = 3$	$t_e = 4$	$t_e = 5$
Activity Domain Area of I	4.3320	4.3320	4.3320	4.3320
Activity Domain Area of u	4.3633	5.1914	5.8164	6.4414
Maximum value of u	1.9267	2.4325	2.9140	3.4004

Table 6: Characteristics of the stabilized solutions in the case of $t_0 = 0$, $\sigma_I = \{1\}$, $A_I = \{1\}$, $x_c = \{(0,0)\}$, $\theta = 0.5$, for different t_e in 2D

Next, we investigate the interaction of the system with external inputs by analyzing Figures 4 and 5, which depict the effects of two distinct stimuli applied at different times.

The Figure 4 illustrates the system's initial response to the applied external input, showing a clear reaction in the field dynamics. By the time we reach the Figure 5, the system has stabilized, and the solutions for both u and v effectively retain the characteristics of both external inputs. In summary, our comprehensive analysis demonstrates that the 2D model successfully captures the dynamics of neural interactions while preserving the essential characteristics of external stimuli across various scenarios. The results pave the way for more sophisticated explorations of neural dynamics in higher-dimensional spaces, providing valuable insights into complex biological systems.

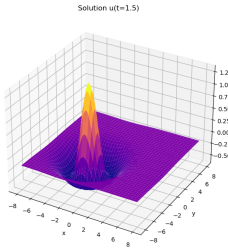


Figure 4: screenshot at $t = 1.5$ so only the external input with center $(-2, -2)$ applied at $t_1 = 0$ during 1 second is represented

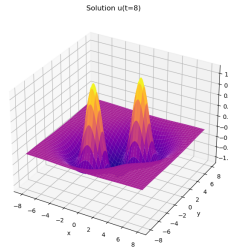
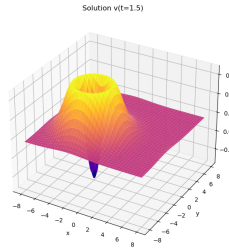
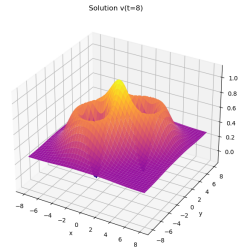


Figure 5: screenshot at $t = 8$ so now both external inputs are represented. The second external input was applied with center $(2, 2)$ at $t_2 = 2$ during 1 second also



4.1 Elliptic Connectivity Function

In neural field models, the characterization of connectivity is vital for understanding information propagation within neural tissues. Traditional isotropic connectivity functions, like Gaussian functions, overlook the complex anisotropic nature of biological systems, where excitatory and inhibitory influences can vary significantly with direction. To model this anisotropic connectivity, we propose an elliptic connectivity function that captures directionally dependent dynamics:

$$\omega_{\text{elliptic}}(x, y) = A_{ex} \exp\left(-\frac{(x_1 - y_1)^2}{2\sigma_{ex,1}^2} - \frac{(x_2 - y_2)^2}{2\sigma_{ex,2}^2}\right) - A_{in} \exp\left(-\frac{(x_1 - y_1)^2}{2\sigma_{in,1}^2} - \frac{(x_2 - y_2)^2}{2\sigma_{in,2}^2}\right) - \omega_{inh}, \quad (13)$$

where A_{ex} and A_{in} are the amplitudes corresponding to excitation and inhibition, and $\sigma_{ex,i}$ and $\sigma_{in,i}$ are the standard deviations of the excitatory and inhibitory components along the respective axes. This formulation allows for enhanced excitatory connectivity along one axis, while inhibition is stronger in the perpendicular direction, creating an elliptic pattern of interaction.

To exemplify the efficacy of this model, we examined a scenario with parameters $A_{ex} = 2$, $A_{in} = 1$, $\sigma_{ex,1} = 1.3$, $\sigma_{ex,2} = 1.0$, $\sigma_{in,1} = 1.8$, $\sigma_{in,2} = 2.0$, and $\omega_{inh} = 0.1$.

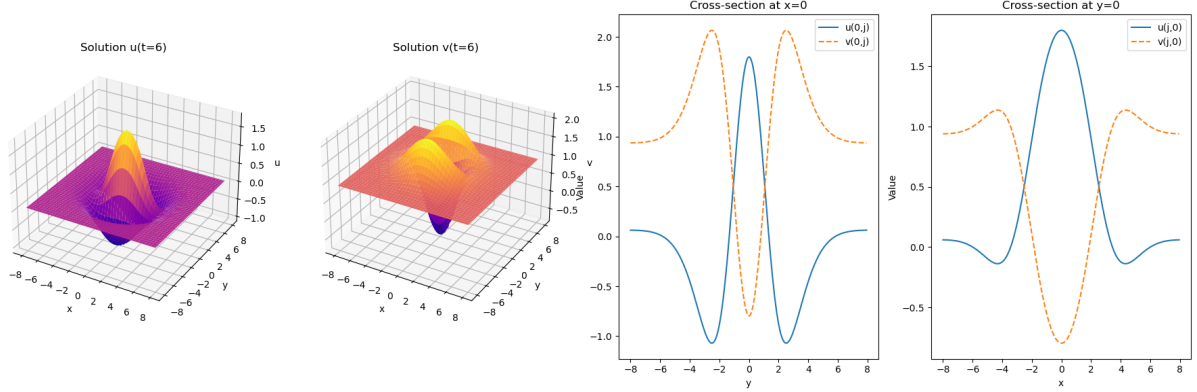


Figure 6: Results obtained using the connectivity function of the form 13 with $\theta = 0.5$ at $t = T = 6$ using scenario 1 with $A_u = 1$, $K = 1$, $\sigma_u = 1$

As illustrated in Figure 6, the results demonstrate that the elliptic connectivity function promotes stronger excitation along the x -axis, while inhibition prevails along the y -axis. This directional preference for signal propagation confirms the model's capability to reflect the intrinsic anisotropic properties of structured neural circuits, providing valuable insights into spatially-dependent neural dynamics.

In summary, the elliptic connectivity function represents a significant advancement over isotropic models by aligning more closely with the physiological realities of neural connectivity, thereby enhancing our understanding of neural processing in regions with structured connectivity.

5 Discussion and Conclusion

This research enhances the understanding of large-scale neural dynamics through the introduction of a two-field model, addressing limitations of traditional single-field approaches. The study investigates the behavior of interconnected neuronal populations and provides insights into how external stimuli influence their dynamics.

Key findings demonstrate that both the amplitude and duration of external stimuli significantly affect the membrane potentials of the neuronal populations. The two-field model effectively captures the distinctive features of externally applied stimuli, highlighting their capability to maintain the integrity of input signals over time, which is crucial for applications involving memory retention and recognition in cognitive processes.

Comparison with the conventional single-field model reveals that the two-field framework preserves characteristics of multiple sequential stimuli, better mimicking real-world neural activities where overlapping signals occur. Additionally, results emphasize the importance of the threshold parameter θ in shaping neuronal activity dynamics. Variations in θ critically influence the final state of the network by

determining which neuronal inputs exceed threshold activity, thus affecting spatial and temporal patterns.

Despite these advancements, the model has limitations, including the assumptions of homogeneity and the simplifications present in the firing rate function. Future work may explore varying connectivity kernels and more complex firing rate functions to enhance biological validity.

Moving forward, the model shows potential for extension into three-dimensional spaces and the inclusion of stochastic dynamics or delay mechanisms, further improving its fidelity to biological processes. Integrating the model with experimental data can provide robust validation and drive the development of applications in neuroscience and cognitive computing.

In conclusion, the two-field neural model represents a significant advancement in simulating large-scale brain activity, offering a valuable foundation for future explorations in neural processing and memory systems. Its ability to accommodate complex stimulus patterns and retain their characteristics paves the way for deeper investigations into neural function and cognition.

Python code

Before the bibliography there's an appendix with the python code developed to numerically approximate the models used in the thesis.

References

- [1] S.L. Amari, Dynamics of pattern formation in lateral-inhibition type neural fields, *Biol. Cybernet.* 27 (2) (1977) 77–87.
- [2] H.R. Wilson and J.D. Cowan, Excitatory and inhibitory interactions in localized populations of model neurons, *Bipophys. J.*, 12 (1972) 1–24.
- [3] S. Coombes, Waves, bumps, and patterns in neural field theories. *Biological Cybernetics*, 93(2005), 91-108.
- [4] Killpatrick, Z. P., & Ermentrout, G. B. (2013). Wandering bumps in stochastic neural fields. *SIAM Journal on Applied Dynamical Systems*, 12(1), 61–94.
- [5] Kuehn, C., & Riedler, M. G. (2014). Large deviations for nonlocal stochastic neural fields. *Journal of Mathematical Neuroscience*, 4(1), 1–28.
- [6] T.Sequeira, Numerical simulations of one- and two-dimensional stochastic neural field equations with delay, Master thesis, Instituto Superior Técnico.
- [7] W. Wojtak, *A novel dynamic field model supporting a continuum of bump amplitudes: Analysis and Applications*, PhD Thesis, Universidade do Minho, <https://drive.google.com/file/d/1so52lwNDnJixVtog7qqXGxMdiq-AcDXK/view>
- [8] W. Wojtak, S. Coombes, D. Avitabile, E.Bicho, W. Erlhagen, A dynamic neural field model of continuous input integration, *Biol. Cybernet.*, 115 (2021) 451–471.
- [9] Wojtak, W., Coombes, S., Avitabile, D. et al. Robust working memory in a two-dimensional continuous attractor network. *Cogn Neurodyn* (2023). <https://doi.org/10.1007/s11571-023-09979-3>
- [10] Lima, P. M., & Buckwar, E. (2012). Numerical solution of the neural field equation in the two-dimensional case. *SIAM Journal on Scientific Computing*, 34(4), B452-B471.
- [11] Avitabile, A. (2014). Numerical approximations of nonlocal equations. *Journal of Computational and Applied Mathematics*, 273, 112-123.